

# BUDGET ANALYSIS OF TURBULENT KINETIC ENERGY IN A TIP-LEAKAGE FLOW OF A SINGLE BLADE: RANS VS ZONAL LES

*J.-F. Monier<sup>1,2</sup> - J. Boudet<sup>2</sup> - J. Caro<sup>2</sup> - L. Shao<sup>2</sup>*

<sup>1</sup>SAFRAN Aircraft Engines, Rond-point René Ravaud, 77550 Moissy-Cramayel, France,  
jean-francois.monier@doctorant.ec-lyon.fr

<sup>2</sup>Univ Lyon, École Centrale de Lyon, CNRS, LMFA, 36, avenue Guy de Collongue, F-69134,  
Écully cedex, France,  
jerome.boudet@ec-lyon.fr, liang.shao@ec-lyon.fr

## ABSTRACT

This study aims at analyzing the modeling of turbulence in a tip-leakage flow. The academic configuration considered is made of a single airfoil and a flat casing, with clearance, at  $Re=9.3e5$ .

For characterising the turbulence, a zonal large-eddy simulation (ZLES), validated against experimental data, is considered as reference. ZLES was previously shown to describe precisely the flow features in the tip region, including the Reynolds stresses.

Two steady Reynolds-averaged Navier-Stokes (RANS) simulations, using Wilcox's  $k-\omega$  model, are evaluated against this reference. The first simulation uses the Boussinesq constitutive relation, whereas the second simulation relies on the quadratic constitutive relation (QCR).

The analysis focuses on the mean velocities, the Reynolds stresses and a term-to-term decomposition of the turbulent kinetic energy budget. RANS is shown to under-estimate the vorticity of the flow, the Reynolds stresses and the turbulent kinetic energy budget terms. The QCR has little effects on these deficits.

## KEYWORDS

TIP-LEAKAGE FLOW, SINGLE AIRFOIL, RANS, LES, REYNOLDS STRESSES, TURBULENT KINETIC ENERGY BUDGET

## NOMENCLATURE

$M$	Mach number	$\Delta x^+, \Delta y^+, \Delta z^+$	Cell sizes at the wall, in wall units
$\mathbf{O}$	Normalized rotation tensor		
$Re_c$	Reynolds number based on the chord length of the blade	$\mathbf{\Pi}$ $\mathbf{\Xi}$	Sub-grid scale stress tensor Numerical residual tensor
$U$	Free-stream velocity	$\delta_{ij}$	Krøeneker symbol
$c$	Chord-length of the blade	$\rho$	Density
$h$	Tip-clearance height	$\boldsymbol{\tau}$	Viscous stress tensor
$k$	Turbulent kinetic energy	$\boldsymbol{\tau}_t \setminus \boldsymbol{\tau}_t^{QCR}$	Reynolds stress tensor with Boussinesq constitutive relation \with QCR
$p$	Pressure		
$u_1, u_2, u_3$	Stream-wise (resp. transverse and span-wise) velocities	$\omega$	Turbulent kinetic energy specific dissipation rate
$x_1, x_2, x_3$	Stream-wise (resp. transverse and span-wise) directions		

## INTRODUCTION

The overall aircraft fleet is expected to be twice as important as today by 2030 (Tucker, 2013). In order to cope with this challenge, the economical and ecological cost of jet engines must be reduced. This is linked with the capacity to reduce their mass and size, *i.e.* increase the pressure ratio, which leads to a worsening of the three dimensional effects such as tip leakage.

The tip leakage flow is partly caused by the pressure difference between the pressure side and the suction side of the blade, at the blade-tip clearance. This secondary flow develops as a large vortex in the blade passage, causing important pressure losses and noise.

The tip leakage has already been investigated numerically using Reynolds-averaged Navier-Stokes (RANS) simulations for more than two decades (with the work of Storer and Cumpsty (1991) for instance, or Borello *et al.* (2006) for high order turbulence models). If these simulations are widely used for conception, they fail to predict correctly some of the unsteady features of the tip-leakage vortex, such as vortex wandering (Boudet *et al.*, 2015a). Their description of turbulence is also questionable. A better description of the tip-leakage flow can be provided by large-eddy simulation (LES), but at a much higher computational cost, preventing its usage for industrial conception.

A Zonal large-eddy simulation (ZLES) from Boudet *et al.* (2016) was validated against experimental results for the mean velocities and the Reynolds stresses. The experiment does not give access to an in-depth characterisation of the turbulence, such as the turbulent kinetic energy budget. For this reason, the ZLES is used as a reference to investigate the turbulence modelling in RANS simulations, in order to understand where they fail to represent correctly the physics. The Reynolds stresses and the turbulent kinetic energy budgets are compared between the LES region of the ZLES and two RANS simulations. These RANS simulations both use the original Wilcox  $k - \omega$  model, but differ on the constitutive relation. The first simulation uses the classical Boussinesq constitutive relation, while the second simulation uses the quadratic constitutive relation (QCR) (Spalart, 2000). This method of analysis was previously applied on a corner separation in a linear cascade (Monier *et al.*, 2016).

## EXPERIMENTAL SET-UP

In order to study the effects of tip-leakage experimentally, an airfoil (NACA5510, chord length: 0.2m, span: 0.19m, thickness: 0.02m and camber: 5%) has been placed inside the potential core of a jet. The airfoil is attached to an end-plate at the top and set above an end-plate at the bottom. The set-up presents a tip-clearance at the bottom, with a  $h = 0.01\text{m}$  clearance height, as shown in figure 1. The tip-clearance height is large ( $h/c = 0.05$ ), compared to what is usually used in industrial compressors. In the original experiment, this choice was lead by acoustic considerations. The gap is large in order to increase the tip-clearance noise with respect to the trailing edge noise. Although the present study does not considers the acoustics, this tip-clearance height has been kept in order to be comparable with the available experimental and ZLES results. The experiment was made at a Reynolds number based on the chord length  $\text{Re}_c = 9.3 \times 10^5$  ( $c = 0.2\text{m}$  and  $U = 70\text{m/s}$ , for a Mach number  $M = 0.2$ ). The simplicity of this configuration allowed a detailed experimental characterisation with advanced measurement techniques. The details of the experimental set-up and results are available in the paper of Jacob *et al.* (2016a,b).

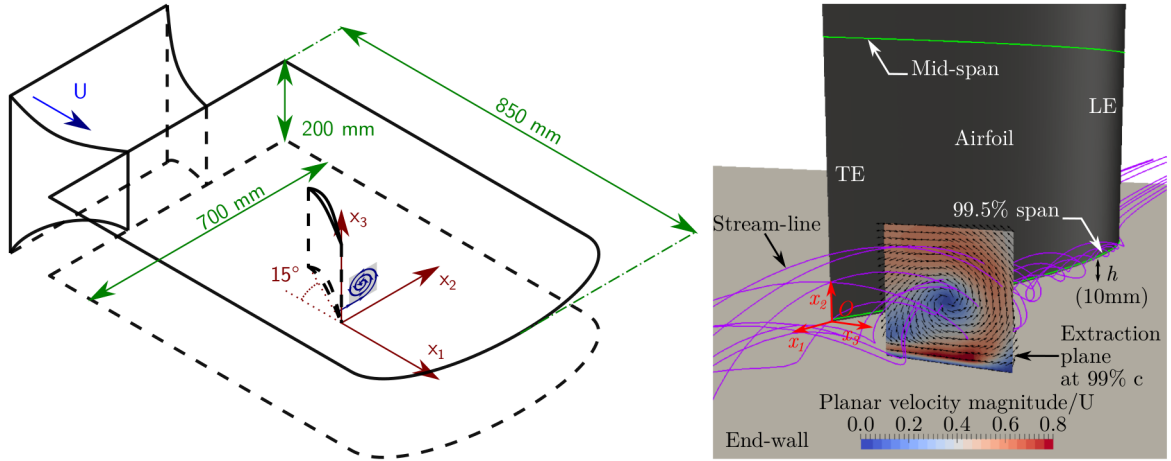


Figure 1: **Representation of the set-up. Left: Experimental set-up. The extraction plane at 99% $c$  is schematically represented in grey. Right: View of the tip region. The origin is set at the top of the tip-gap, at the trailing edge.**

## NUMERICAL METHODS

The simulations have been carried-out with the code *Turb'Flow*, an in-house code of the LMFA described in Boudet *et al.* (2007). It is based on a finite volume solver for the compressible Navier-Stokes equations, on multi-block structured grids.

### Notations

In order to be entirely explicit, the symbols for the ensemble average and for the low frequency filter are kept in the equations. The ensemble average of a quantity  $\varphi$  is noted  $\langle \varphi \rangle$ , the Favre ensemble average is noted  $[\varphi]$ , the low frequency filter is noted  $\bar{\varphi}$  and the Favre low frequency filter is noted  $\tilde{\varphi}$ . The fluctuating part of the low-frequency filtered quantity is noted  $\varphi'$  ( $\bar{\varphi} = \langle \bar{\varphi} \rangle + \varphi'$ ) and the Favre fluctuating part of the Favre low frequency filtered quantity is noted  $\varphi''$  ( $\tilde{\varphi} = [\tilde{\varphi}] + \varphi''$ ). The Favre fluctuating part for RANS is also noted  $\varphi''$  ( $\varphi = [\varphi] + \varphi''$ ) to have a common notation for the Reynolds stresses. Einstein's sum notation is used in this paper.

The coordinate system is the same as in the experiment presented in figure 1. The origin is placed at the blade trailing edge, at the top of the clearance, so the tip-clearance is at  $x_3 \leq 0$ .

### Zonal large-eddy simulation (ZLES)

#### Numerical parameters

The simulation is made for an angle of attack of  $15^\circ$ . The Zonal LES relies on LES around the tip-clearance and RANS in the outer region. A complete explanation of this zonal formulation can be found in Boudet *et al.* (2015a). The LES part relies on the shear-improved Smagorinsky model (SISM) from L ev eque *et al.* (2007) while the RANS part relies on the original Wilcox  $k - \omega$  model (Wilcox, 1988). The cut-off frequency of SISM is set to 630Hz ( $1.8U/c$ ).

The computational domain is over  $29c$  axially,  $37c$  laterally and  $1c$  span-wise, with a grid counting  $150 \times 10^6$  points (split into 524 domains). The grid resolution is  $\Delta x^+ \leq 80$  stream-

wise,  $\Delta y^+ \leq 1.5$  wall-normal and  $\Delta z^+ \leq 30$  cross-stream in the LES area, and all the wall are set to a non-slip adiabatic condition. The boundary-layers are well resolved.

The interpolation of the inviscid fluxes uses a four-point centered scheme from Jameson *et al.* (1981) with a fourth order artificial viscosity in the LES region (coefficient  $\leq 0.03$ , cf. (Boudet *et al.*, 2015b)). The artificial viscosity is increased in the outer (RANS) regions. The viscous flux interpolation uses a two-point centered scheme. The time scheme is explicit, using a three-step Runge-Kutta scheme, with a constant imposed time step of  $1.6 \times 10^{-8}$ s ( $5.6 \times 10^{-6}c/U$ ).

### Turbulent kinetic energy budget

The Reynolds stresses extracted from the LES region are computed as follows:

$$\boldsymbol{\tau}_t = -\langle \bar{\rho} \mathbf{u}'' \otimes \mathbf{u}'' \rangle \quad (1)$$

A budget can be extracted for each Reynolds stress component, with the method of Gao (2014). Then, the turbulent kinetic energy (TKE) budget can be deduced by summation of the diagonal terms of the Reynolds stress tensor ( $k = 1/2 u_i'' u_i''$ ). The TKE budget is theoretically balanced, but practically a residual is present. In order to take into account the effects of this residual, a numerical residual term ( $\Xi$ ) is added to the TKE budget to close it. The TKE budget is expressed as follows:

$$\begin{aligned} \frac{\partial \langle \bar{\rho} k \rangle}{\partial t} = 0 = & \underbrace{-\frac{\partial}{\partial x_j} (\langle \bar{\rho} k \rangle [\tilde{u}_j])}_{\text{Advection}} - \underbrace{\langle \bar{\rho} u_i'' u_j'' \rangle \frac{\partial [\tilde{u}_i]}{\partial x_j}}_{\text{Production}} - \underbrace{\frac{\partial}{\partial x_j} (\langle \bar{\rho} k u_j'' \rangle)}_{\text{Turbulent diffusion}} - \underbrace{\frac{\partial \langle u_i'' p' \rangle}{\partial x_i}}_{\text{Pressure diffusion}} + \underbrace{\left\langle p' \frac{\partial u_i''}{\partial x_i} \right\rangle}_{\text{Pressure dilatation}} \\ & - \underbrace{\langle u_i'' \rangle \frac{\partial \langle \bar{p} \rangle}{\partial x_i}}_{\text{Viscous diffusion}} + \underbrace{\frac{\partial \langle \bar{\tau}_{ij} u_i'' \rangle}{\partial x_j}}_{\text{Viscous dissipation}} - \underbrace{\left\langle \frac{\bar{\tau}_{ij} \partial u_i''}{\partial x_j} \right\rangle}_{\text{SGS diffusion}} + \underbrace{\frac{\partial \langle \bar{\Pi}_{ij} u_i'' \rangle}{\partial x_j}}_{\text{SGS Dissipation}} - \underbrace{\left\langle \frac{\bar{\Pi}_{ij} \partial u_i''}{\partial x_j} \right\rangle}_{\text{SGS Dissipation}} + \underbrace{\Xi_{ii}}_{\text{Numerical residual}} \quad (2) \end{aligned}$$

In order to compare the LES TKE budget with the  $k$  equation of the Wilcox original  $k - \omega$  model, some terms are grouped. Production and numerical residual are kept alone. The viscous dissipation and the SGS dissipation are summed into the dissipation term. All the other terms are summed to form the transport term. The statistics involved in the budgets are computed over 28.57ms ( $10c/U$ ), with a sample every 0.048ms (every 3000 iterations).

## **Reynolds-averaged Navier-Stokes simulations (RANS)**

### Numerical parameters

The RANS simulations are also carried out with Turb'Flow. The computational domain is over  $12.3c$  axially,  $20c$  laterally and  $1c$  span-wise, with a grid counting  $5.4 \times 10^6$  points. The boundary-layers are well resolved, with  $\Delta y^+ \leq 1.5$ , and all the wall are set to a non-slip adiabatic condition.

The interpolation of the inviscid fluxes uses a two-point centered Jameson scheme, with a second order artificial viscosity (coefficient: 0.02), and with an upwind scheme for the turbulence equations. The viscous flux interpolation uses a two-point centered scheme. The time scheme is explicit, using a three-step Runge-Kutta scheme, with a CFL number of 0.6.

### Turbulence modelling

Both RANS simulations use the original Wilcox  $k - \omega$  model (Wilcox, 1988). The first simulation relies on the classical Boussinesq constitutive relation, expressed as follows:

$$\tau_{t,ij} = \mu_t \left( \frac{\partial [u_i]}{\partial x_j} + \frac{\partial [u_j]}{\partial x_i} - \frac{2}{3} \delta_{ij} \frac{\partial [u_k]}{\partial x_k} \right) - \frac{2}{3} \delta_{ij} \langle \rho \rangle [k] \quad (3)$$

$$\mu_t = \langle \rho \rangle \frac{[k]}{[\omega]} \quad (4)$$

The Boussinesq constitutive relation is known to poorly represent anisotropy, and this can be a major drawback in three-dimensional flows such as tip-leakage. In order to add some anisotropy in the Reynolds stress tensor, Spalart (2000) proposed a correction to the Boussinesq constitutive relation that takes into account the vorticity of the flow (see Mani *et al.* (2013) for the compressible formulation). The formulation of the quadratic constitutive relation is:

$$\tau_{t,ij}^{QCR} = \tau_{t,ij} - c_{QCR} (O_{ik} \tau_{t,jk} + O_{jk} \tau_{t,ik}) \quad (5)$$

with  $\tau_t$  the Reynolds stress tensor from the Boussinesq constitutive relation (eq.(3)),  $c_{QCR} = 0.3$  and  $\mathbf{O}$  is the normalised rotation tensor:

$$O_{ij} = \frac{\frac{\partial [u_i]}{\partial x_j} - \frac{\partial [u_j]}{\partial x_i}}{\sqrt{\frac{\partial [u_k]}{\partial x_l} \frac{\partial [u_k]}{\partial x_l}}} \quad (6)$$

In both cases, the TKE budget ( $k$  equation) is the following:

$$\frac{\partial \langle \rho \rangle [k]}{\partial t} = 0 = \underbrace{\langle \tau_{t,ij} \rangle \frac{\partial [u_i]}{\partial x_j}}_{\text{Production}} - \underbrace{\frac{\partial \langle \rho \rangle [k] [u_j]}{\partial x_j}}_{\text{Advection}} + \underbrace{\frac{\partial}{\partial x_j} \left( \mu \frac{\partial [k]}{\partial x_j} \right)}_{\text{Molecular diffusion}} + \underbrace{\frac{\partial}{\partial x_j} \left( \frac{\mu_t}{\sigma_k} \frac{\partial [k]}{\partial x_j} \right)}_{\text{Turbulent transport \& pressure diffusion}} - \underbrace{c_k \langle \rho \rangle [k] [\omega]}_{\text{Dissipation}} + \underbrace{\Xi_{ii}}_{\text{Numerical residual}} \quad (7)$$

with  $c_k = 0.09$  and  $\sigma_k = 2.0$ . To simplify the comparison, the three terms accounting for transport (the advection term, the molecular diffusion term and the turbulent transport & pressure diffusion term) are summed into a single transport term. A numerical residual term is also calculated and added to the right-hand side to close the budget.

### **PRESSURE COEFFICIENT**

The pressure coefficient is computed at 50% span height and 99.5% span height (*i.e.* at  $0.1h = 1\text{mm}$  from the blade tip). It is presented in figure 2.

The ZLES and both RANS simulations present a good agreement on the pressure coefficient, for both the mid-span and the tip extractions. At mid-span, the pressure coefficient is comparable to a compressor blade pressure coefficient. The RANS with Boussinesq constitutive relation overestimates the pressure coefficient at the leading edge stagnation point, and so does the RANS with QCR. At 99.5% span, the pressure coefficient presents a slightly different

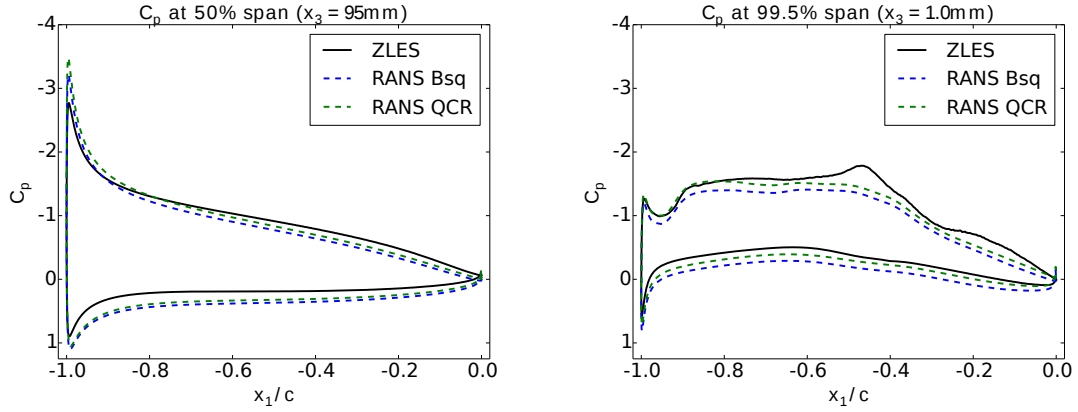


Figure 2: **Pressure coefficient on the blade. Left: mid-span (95mm from the blade tip), right: 99.5% of the span (0.1h or 1mm from the blade tip).  $x_1/c = -1$  represents the leading edge and  $x_1/c = 0$  the trailing edge.**

topology. The pressure difference between the pressure side and the suction side is globally less important, but instead of monotonously decreasing along the chord, an increase of pressure difference is visible at  $x_1/c \approx -0.45$ . This is due to the increase of the depression on the suction side, due to the presence of the jet leakage. The RANS simulations slightly underestimate the depression.

## MEAN VELOCITIES

The ZLES was validated against experimental results in Boudet *et al.* (2016), for the mean velocities and the Reynolds stresses. In the present paper, the ZLES is used as reference to analyse the RANS results. The mean velocities are extracted on a constant  $x_1$  plane, at 99% of the chord, as presented schematically in figure 1. The velocities are presented in figure 3.

With respect to the ZLES, the mean velocities calculated by both RANS simulations present a similar topology, but with differences on the intensity. While the ZLES simulation shows a highly vortical flow, the RANS simulations present a flow rotating more slowly, with a diffused vortex. The RANS prediction for the center of the vortex is correct, even if it is located a little bit upper than in the ZLES. The effect of the QCR is negligible on the mean velocities.

## REYNOLDS STRESSES

The Reynolds stresses are a measure of the effects of turbulence in ZLES, and a measure of the quality of the modelling in the RANS simulations. Both normal and shear stresses are investigated. The Reynolds stresses are extracted on the same constant  $x_1$  plane, at 99% of the chord. The normal stresses are plotted on figure 4 and the shear stresses are plotted on figure 5. All the stresses are normalized by  $\rho U^2$ . For the sake of clarity, the scaling of each figure is Reynolds stress dependant.

For the three normal stresses, two areas of high intensity can be seen in the ZLES simulation. The first area is at the bottom left of the figure ( $x_3 \approx -3\text{mm}$ ), where a jet comes from the pressure side of the blade through the tip-clearance. The second area is on the border of the vortex, and depends on the stress. The first stress  $\langle u_1''u_1'' \rangle$  is globally intense all around the vortex, while the other ones are more localised. The second stress  $\langle u_2''u_2'' \rangle$  has a peak of intensity

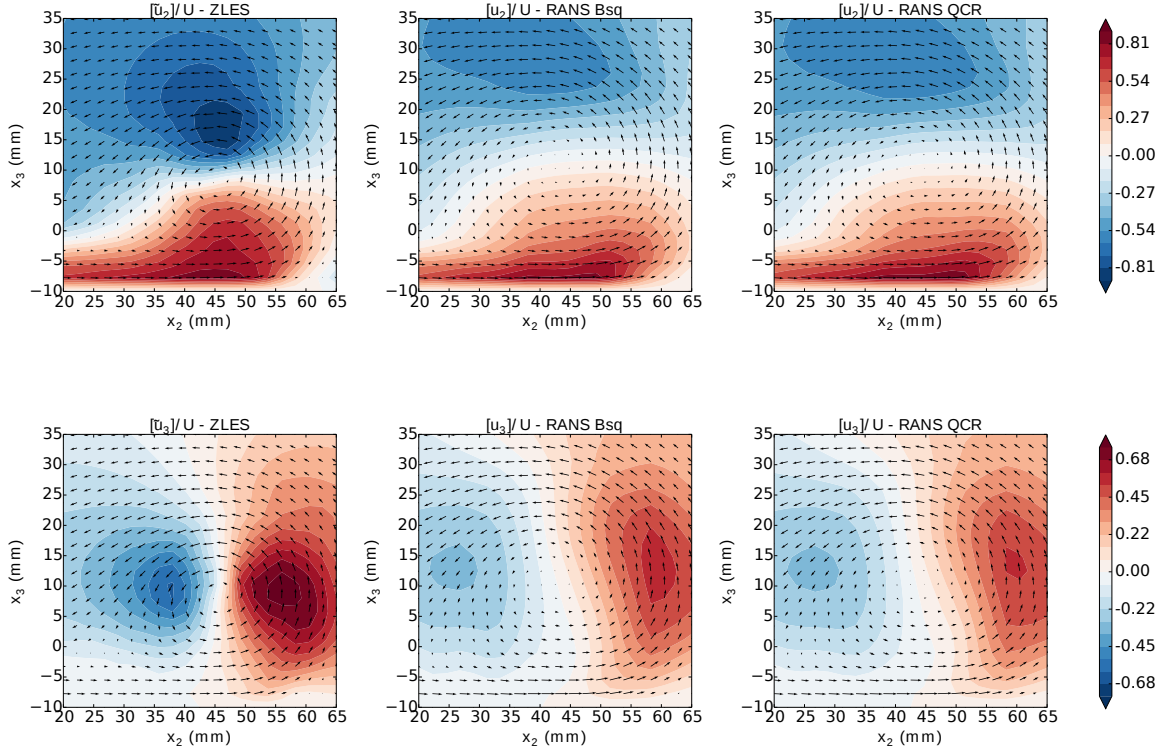


Figure 3: Mean velocities: transverse (upper row) and span-wise (lower row) components. Left: ZLES, middle: RANS-Boussinesq, right: RANS-QCR. The arrows represent the local velocity on the plane.

close to  $x_2 = 60\text{mm}$  and  $x_3 = -7\text{mm}$ , while the third stress  $\langle u_3''u_3'' \rangle$  has its peak at  $x_2 = 58\text{mm}$  and  $x_3 = 20$ . For the RANS simulations, the normal Reynolds stresses are much less intense than in the ZLES. The most intense regions of the ZLES are partly described by RANS, with a lower intensity: the jet for the three components, the bottom right region for the second component and the top right region for the third component. These last two regions are barely visible in RANS. The QCR increases a little the first and second stresses, but it is far from enough to have comparable levels with ZLES. The normal Reynolds stresses are clearly under-predicted by both RANS simulations, compared to the ZLES.

In the particular case of an isotropic flow, the shear stresses are null. Consequently the shear Reynolds stresses can measure the anisotropy level of the flow. In figure 5, the shear Reynolds stresses follow similar trends as the normal Reynolds stresses, for the ZLES and the RANS simulations. The areas of higher intensity are placed for the ZLES in the jet and on the border of the vortex, but also in its center. The values are significant, which demonstrates the anisotropy of this flow. Conversely, the RANS simulations show very weak shear Reynolds stresses. The main area of these stresses is in the jet, for both simulations. It is not possible to conclude if the weakness of the shear stresses, compared to the ZLES, is due to the difficulties RANS two-equation models are known to have when the flow is anisotropic, or if it is due to the diffusion of the vortex, observed in figure 3. The QCR was expected to add anisotropy to the Reynolds stresses, but its effect appears not significant.

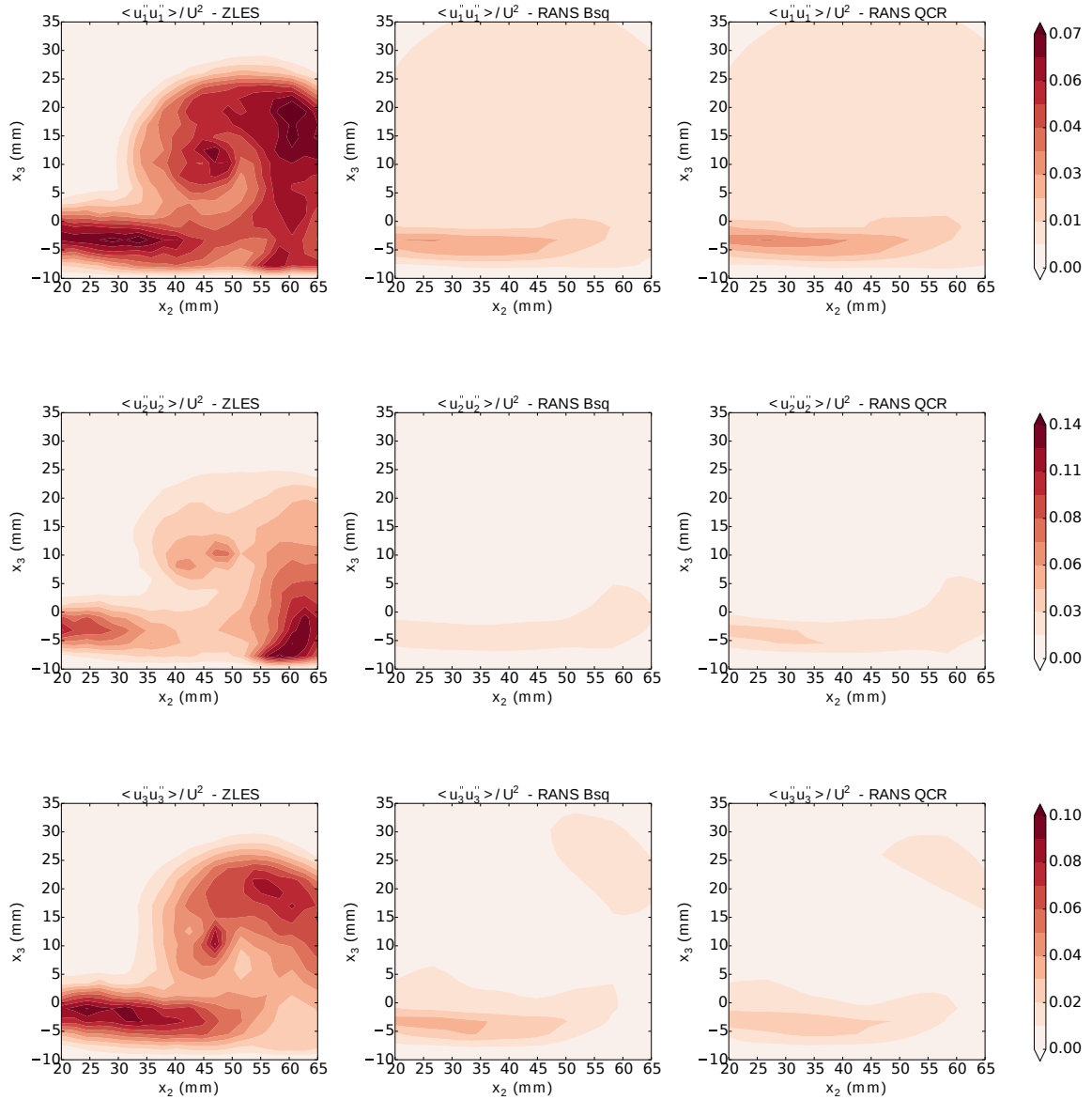


Figure 4: Normal Reynolds stresses. Left: ZLES, middle: RANS-Boussinesq, right: RANS-QCR.

## TURBULENT KINETIC ENERGY BUDGET

The turbulent kinetic energy budget accounts for the phenomena of production, dissipation and transport of the turbulent kinetic energy. For RANS, it is used to evaluate the capacity of the models to represent accurately the physics locally. In the  $k - \omega$  models considered in this study, it corresponds to the transport equation of  $k$ . The TKE budget terms are extracted on the same plane as the Reynolds stresses, and presented in figure 6. All the terms are normalised by  $\rho_{\text{ref}}^2 \times U^4 / (\mu_{\text{ref}} \times 10^6)$ , with  $\rho_{\text{ref}} = 1.117 \text{kg.m}^{-3}$  and  $\mu_{\text{ref}} = 1.81 \times 10^{-5} \text{kg.m}^{-1}.\text{s}^{-1}$ .

The numerical residual term is used to gauge the closure of the TKE budget. This term accounts for all the numerical effects, such as artificial viscosity effects or mesh dissipation. In the ZLES case, the term can be positive or negative, and seems roughly opposed to the transport

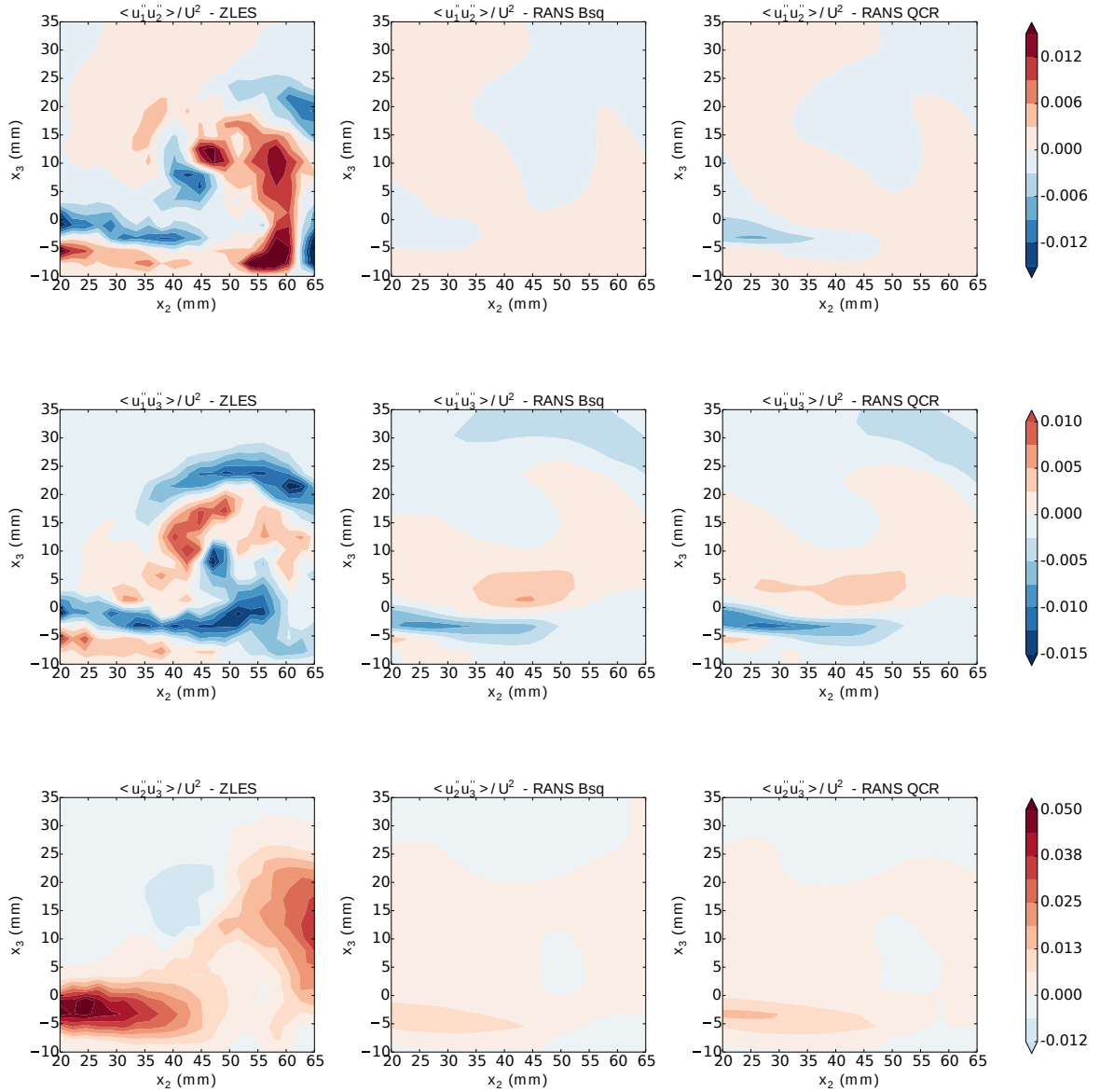


Figure 5: Shear Reynolds stresses. Left: ZLES, middle: RANS-Boussinesq, right: RANS-QCR.

term. It is far from being negligible, but seems essentially to counter-part the spatial oscillations of the transport term, while the patterns of the production term and dissipation term are not visible. This can be an effect of the insufficient statistical convergence of the transport term, which relies on many double and triple correlations. For the physical budget terms (production, dissipation and transport), the areas where the residual is locally more than half as important as the term considered are striped, in order to map the areas where a physical analysis is not significant. The RANS simulations show a small amount of numerical residual because the  $k$ -equation is directly solved. The most intense residuals are opposed again to the transport term close to the end-wall. In that case, the reason could be an important mesh size variation.

The production term of the TKE budget accounts for the turbulent kinetic energy creation.

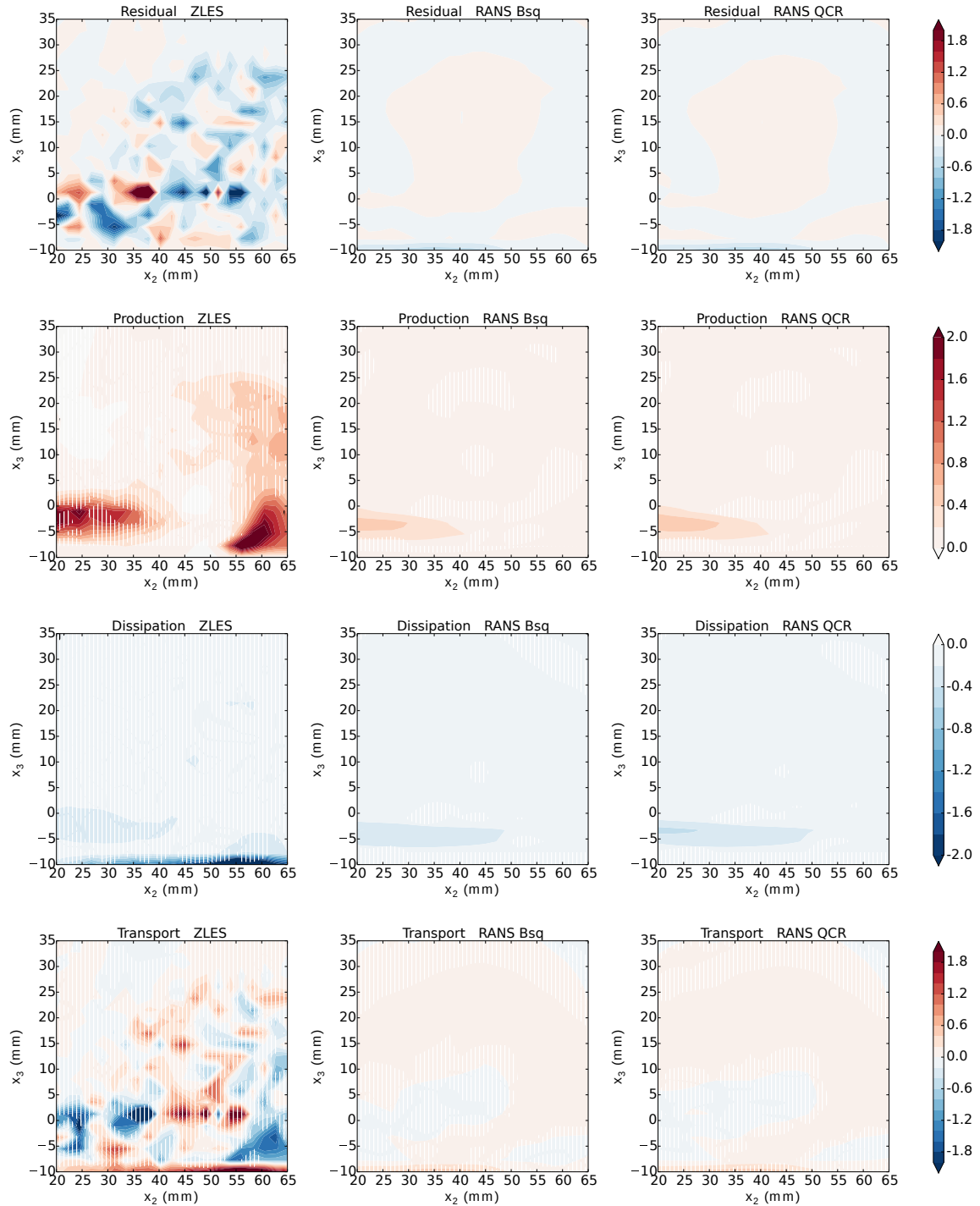


Figure 6: **Turbulent kinetic energy budget. Left: ZLES, middle: RANS-Boussinesq, right: RANS-QCR. The regions where the numerical residual is more than half the term considered are striped.**

The main areas of production for the ZLES simulation are the jet and around  $x_2 = 60$  mm and  $x_3 = -7$  mm. Those areas correspond to regions of high intensity for both the normal

Reynolds stresses and the shear Reynolds stresses, as presented in figure 4 and figure 5. In the second area, around  $x_2 = 60\text{mm}$  and  $x_3 = -7\text{mm}$ , the production is believed to be an effect of the interaction between the tip-leakage vortex and the end-wall boundary-layer (Tan *et al.*, 2015). The important production area in the jet is impacted by the high residual, but not entirely, while the other area of important production is not significantly impacted by the high residual. Concerning the RANS simulations, the main area of production is in the jet, but with levels ten times smaller than for the ZLES. The second area of production is not visible in the RANS results. As could be expected, the global under-prediction of the Reynolds stresses is associated with an under-prediction of the turbulent kinetic energy production. The QCR still do not have a significant effect on the results.

The dissipation term of the TKE budget accounts for the turbulent kinetic energy damping. The main area of dissipation for the ZLES is close to the end-wall, at  $x_3 < -7\text{mm}$ . No significant dissipation can be seen in the jet area or in the vortex area, where the production mainly takes place. The area of important dissipation is not affected by the high numerical residual. For the RANS simulations, the dissipation occurs in the jet, where the production is intense. The chosen scaling does not allow to see the dissipation at the wall in RANS, due to the weakness of the term. This is a classical issue in RANS, the production and dissipation are superimposed, with a small amount of transport (Wilcox, 2006). This behaviour is not corrected by the use of the QCR.

The transport term of the TKE budget accounts for the turbulent kinetic energy displacement in the flow. For the ZLES, as already pointed out, the transport term shows strong oscillations, in opposition with the numerical residual term. This seems to be due to an insufficient statistical convergence. However, the region in the bottom right of the figure shows values sufficiently intense compared to the residual, and can be analysed. An important area of positive energy transportation is found in the area of high dissipation, near the end-wall. Energy is taken from the vortex (negative transport) and transferred to the end-wall (positive transport) where it is dissipated. The RANS simulations show a small amount of transport, but it is not negligible compared to the other terms. However, the area of high intensity for this term is under the jet, near the end-wall, which is not really physical, due to the absence of balance of the TKE budget it infers. The QCR yields no significant effect again.

## CONCLUSIONS

A detailed ZLES simulation of a tip-leakage flow, validated against experimental data in Boudet *et al.* (2016), has been used as a reference to analyse RANS simulations. ZLES is physically conclusive concerning the turbulence, for both the Reynolds stresses and the turbulent kinetic energy budget. A significant numerical residual of the TKE can be found, probably due to a lack of statistical convergence of the triple correlations (transport term), but this does not affect the main regions of interest.

The RANS simulations fail to represent correctly the mean velocities, over-estimating the vortex diffusion. In the section considered, the levels of all the Reynolds stresses are too small compared to the ZLES Reynolds stresses. It is not possible to conclude if the wrong prediction is due to the important diffusion of the vortex, lowering the turbulence levels, the imprecision of the turbulence models, or a cumulation of the two effects. The turbulent kinetic energy budgets show a classical issue in RANS, with production and dissipation superimposed. The transport term creates a numerical residual close to the end-wall, for reasons that are not well understood yet. The QCR addition of anisotropy to the Reynolds stresses is driven by the vorticity of the

flow. In a highly vortical tip-leakage flow, the QCR was expected to modify significantly the Reynolds stresses. However, the QCR yields no significant impact on the results.

The present paper is not exhaustive, and additional analyses can be done to compare the RANS and ZLES. Among these are the losses inside the tip-leakage vortex, or traverses for a more quantitative analysis of some of the data presented in this paper. These analyses are ongoing.

## ACKNOWLEDGEMENTS

This study was supported by the Franco-Chinese project VortexFlowCFD, co-funded by SAFRAN Aircraft Engines and the French National Research and Technology Agency (ANRT).

The simulations were performed using HPC resources from GENCI-CINES (Grant c2016-2a5039).

## REFERENCES

- Borello, D., Rispoli, F., and Hanjalic, K. (2006). Prediction of Tip-Leakage Flow in Axial Flow Compressor with Second Moment Closure. In *ASME Turbo Expo 2006: Power for Land, Sea, and Air*, pages 271–281. American Society of Mechanical Engineers.
- Boudet, J., Cahuzac, A., Kausche, P., and Jacob, M. C. (2015a). Zonal Large-Eddy Simulation of a Fan Tip-Clearance Flow, With Evidence of Vortex Wandering. *Journal of Turbomachinery*, 137(6):061001.
- Boudet, J., Caro, J., Shao, L., and L ev eque, E. (2007). Numerical studies towards practical large-eddy simulation. *Journal of Thermal Science*, 16(4):328–336.
- Boudet, J., Monier, J. F., and Gao, F. (2015b). Implementation of a roughness element to trip transition in large-eddy simulation. *Journal of Thermal Science*, 24(1):30–36.
- Boudet, J. C., Li, B., Caro, J., Jondeau, E., and Jacob, M. C. (2016). Tip-Leakage Flow: a Detailed Simulation with a Zonal Approach. 22<sup>nd</sup> AIAA/CEAS Aeroacoustics conference, paper AIAA-2016-2824.
- Gao, F. (2014). *Advanced numerical simulation of corner separation in a linear compressor cascade*. PhD Thesis, Ecole Centrale de Lyon, Ecully.
- Jacob, M. C., Jondeau, E., and Li, B. (2016a). Time-resolved PIV measurements of a tip leakage flow. *International Journal of Aeroacoustics*, pages 662–685.
- Jacob, M. C., Jondeau, E., Li, B., and Boudet, J. C. (2016b). Tip Leakage Flow: Advanced Measurements and Analysis. 22<sup>nd</sup> AIAA/CEAS Aeroacoustics conference, paper AIAA-2016-2823.
- Jameson, A., Schmidt, W., Turkel, E., and others (1981). Numerical solutions of the Euler equations by finite volume methods using Runge-Kutta time-stepping schemes. *AIAA paper*, 1259:1981.
- L ev eque, E., Toschi, F., Shao, L., and Bertoglio, J.-P. (2007). Shear-improved Smagorinsky model for large-eddy simulation of wall-bounded turbulent flows. *Journal of Fluid Mechanics*, 570:491.

- Mani, M., Babcock, D., Winkler, C., and Spalart, P. (2013). Predictions of a Supersonic Turbulent Flow in a Square Duct. American Institute of Aeronautics and Astronautics.
- Monier, J.-F., Gao, F., Boudet, J., Shao, L., and Lu, L. (2016). Budget analysis of turbulent kinetic energy in corner separation : RANS VS LES. In *Proceedings of the European Conference on Computational Fluid Dynamics, June 5-10, 2016*. European Community on Computational Methods in Applied Sciences (ECCOMAS).
- Spalart, P. R. (2000). Strategies for turbulence modelling and simulations. *International Journal of Heat and Fluid Flow*, 21(3):252–263.
- Storer, J. A. and Cumpsty, N. A. (1991). Tip Leakage Flow in Axial Compressors. *Journal of Turbomachinery*, 113(2):252.
- Tan, D., Li, Y., Wilkes, I., Miorini, R. L., and Katz, J. (2015). Visualization and Time-Resolved Particle Image Velocimetry Measurements of the Flow in the Tip Region of a Subsonic Compressor Rotor. *Journal of Turbomachinery*, 137(4):041007.
- Tucker, P. (2013). *Unsteady Computational Fluid Dynamics in Aeronautics*, volume 104. Springer Science & Business Media.
- Wilcox, C., D. (1988). Reassessment of the scale-determining equation for advanced turbulence models. *AIAA Journal*, 26(11):1299 – 1310.
- Wilcox, D. C. (2006). *Turbulence Modeling for CFD*. D C W Industries, La Cañada, Calif, 3rd edition edition.